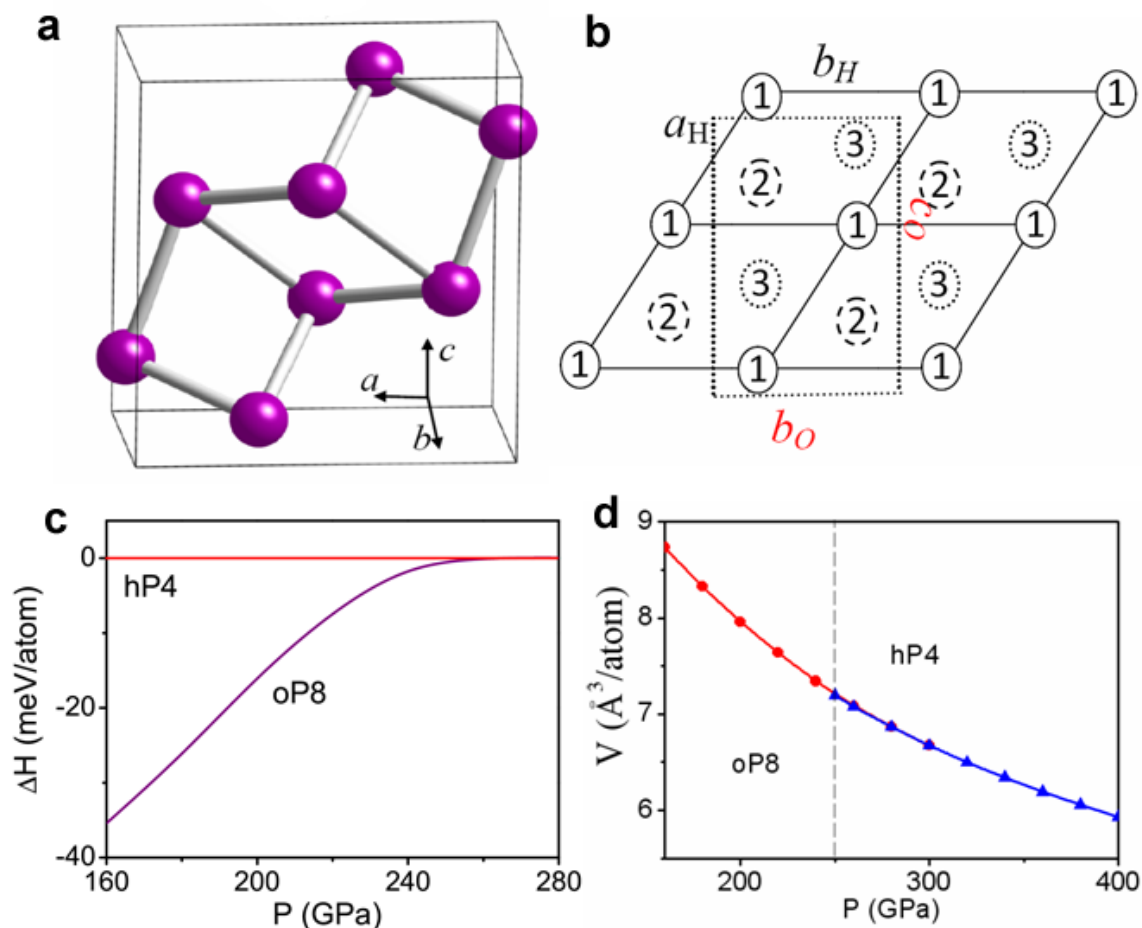


**Figure S1 | Transparent sodium.** The photograph of transparent sodium sample taken in transmitted and reflected light (**a**) and in reflected light only (**b**) at 186 GPa. The transparent sample was created at 194 GPa, but pressure stabilizes at 186 GPa. The sample is squeezed between a pair of diamond anvils inside rhenium gasket. The diameter of culet of diamond anvil is 40  $\mu\text{m}$ , and size of the sample is  $\approx 5\text{-}8\ \mu\text{m}$ . **c**, Optical absorption spectrum from this sample ( $E$  is photon energy,  $\alpha$  is absorption coefficient and  $d$  is sample thickness). It was determined from the ratio of the transmitted light to the reference spectrum taken with the same field diaphragm but without the pressure cell. The sample thickness was estimated as  $d \approx 3\text{-}5\ \mu\text{m}$ , with the initial thickness of 8  $\mu\text{m}$ . Breaks in the spectrum are due to regions of complete absorption by Notch filters in the experimental setup. The red line is shown as a visual guide. The nearly linear dependence in these coordinates indicates direct gap allowed optical transitions in agreement with theory (Fig. 4b). The theoretical Raman spectrum (orange line) for the oP8 structure at 140 GPa is compared with the experimental results (black and green lines) in the pressure range of 139-142 GPa shown in **d**. The Raman measurements were limited by frequencies larger than 220  $\text{cm}^{-1}$ . Raman intensities are computed from the second-

order derivative of the electronic density matrix with respect to a uniform electric field, using the Quantum-ESPRESSO package (S. Baroni, *et al.* <http://www.pwscf.org/>).



**Figure S2 | Crystal structure of oP8 phase and its relation with Na-hP4.** **a**, Crystal structure of the oP8 phase. At the theoretical pressure of 230 GPa, lattice parameters:  $a = 4.248 \text{ \AA}$ ,  $b = 2.829 \text{ \AA}$ , and  $c = 4.992 \text{ \AA}$ ; atoms occupy two inequivalent  $4c$  sites: Na1 (0.487, 0.25, 0.296) and Na2 (0.3085, 0.25, 0.9193). **b**, Top view along the  $c$ -axis within  $(2a \times 2b)$  plane of Na-hP4. Labels 1, 2, and 3 denote the atoms occupying the C, A, and B layers in the Fig. 4a, respectively. oP8 unit cell is represented by the dotted rectangle with the lattice parameters  $a_O = c_H$ ,  $b_O = b_H$ , and  $c_O = 3^{1/2} a_H$ , where  $a_H$ ,  $b_H$ , and  $c_H$  are the lattice parameters of Na-hP4. In the oP8 structure, Na atoms are slightly shifted in the  $ab$  plane for atoms belonging to the C layers and along the  $c$ -axis

for atoms comprising the A and B layers relative to the more symmetric positions in Na-hP4. Therefore, the oP8 structure can be viewed as a small distortion of Na-hP4 and the nearly perfect h.c.p arrangement of interstitials in Na-hP4 also applies to the oP8 structure. The oP8→hP4 transition, predicted at about 250 GPa, is second order, as characterized by the merging of two enthalpy curves (c) and the continuous equation of states (d).

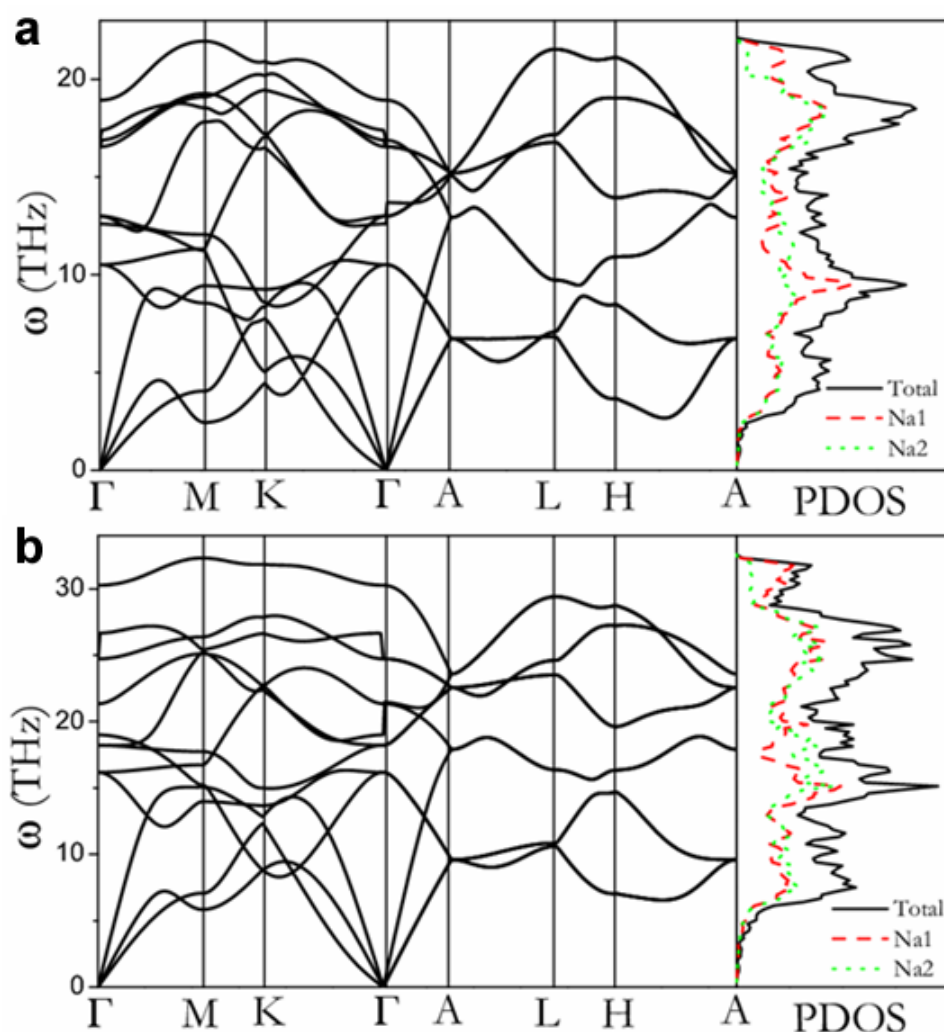


**Figure S3 | Phonon dispersion curves and projected vibrational density of states for Na-hP4 at the volumes of (a)  $6.67 \text{ \AA}^3/\text{atom}$  ( $\sim 300 \text{ GPa}$ ) and (b)  $5.03 \text{ \AA}^3/\text{atom}$  ( $\sim 600 \text{ GPa}$ ).** The pressure values in parentheses are from theory. Phonons were calculated by the supercell method (program PHON by D. Alfè, available at <http://chianti.geol.ucl.ac.uk/~dario>, 1998), the force constants matrix being determined by

VASP using a  $2 \times 2 \times 2$  cell and a  $4 \times 4 \times 3$   $k$  mesh. The dynamical stability of Na-hP4 is thus validated by the phonon calculations in view of the absence of any imaginary phonon frequencies.

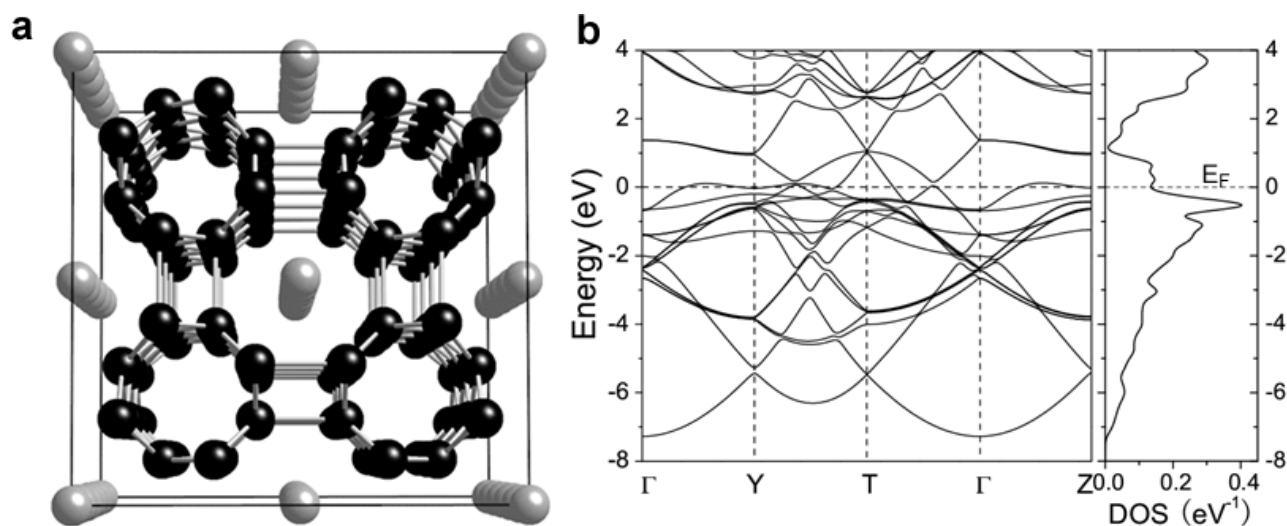


**Figure S4 | Structural and electronic properties of tI19 phase.** **a**, Structural approximant for the incommensurate host-guest composite tI19 phase used in the enthalpy calculation and **b**, its electronic bandstructure and total density of states at the volume of  $7.27 \text{ \AA}^3/\text{atom}$ . For tI19 structure at 130 GPa, the host and guest tetragonal body-centered lattice parameters are  $a_H = a_G = 7.0883 \text{ \AA}$ ,  $c_H = 3.483 \text{ \AA}$ , and  $c_G = 2.11 \text{ \AA}$  taken from Ref. 8 (Gregoryanz, E. *et al.*). The  $c_H/c_G$  ratio of  $3.48/2.11$  approximately equals to  $1.667$  ( $5/3$ ). Therefore the periodic approximant was constructed by incorporating the  $1 \times 1 \times 5$  supercell of guest lattice into  $1 \times 1 \times 3$  supercell of host lattice. The calculated electronic density of states at Fermi level is  $0.136 \text{ states}/(\text{eV} \cdot \text{atom})$ , much smaller than that ( $0.489 \text{ states}/(\text{eV} \cdot \text{atom})$ ) of the bcc phase at ambient pressure. This suggests that tI19 phase is a relatively weak metal. We note that the electronic behavior of the tI19 phase does not change significantly within its stability field.

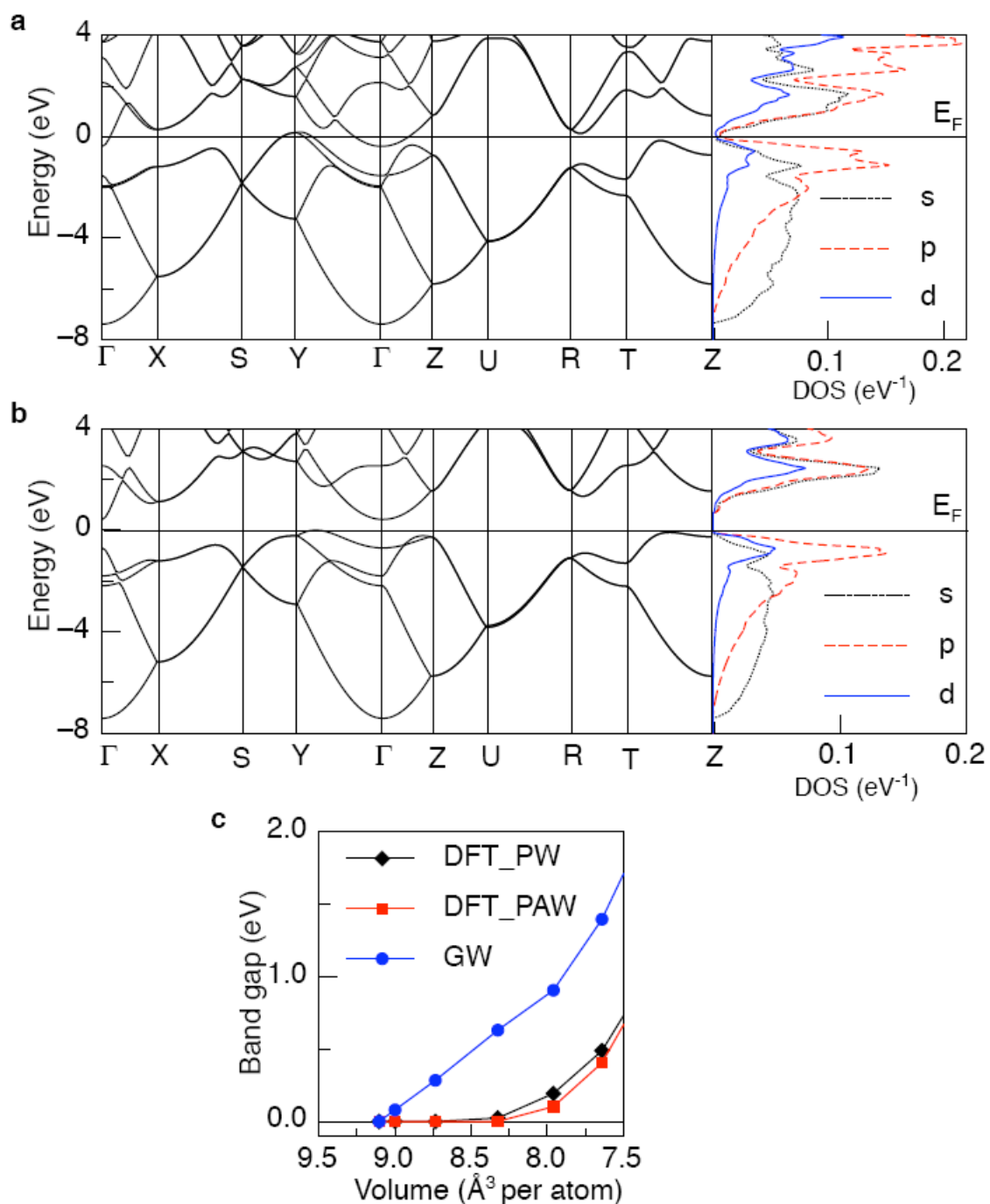


**Figure S5 | Electronic properties of oP8 phase.** Band structure and projected density of states plots at the volume of (a) 9.21 Å<sup>3</sup>/atom (~140 GPa) and (b) 7.64 Å<sup>3</sup>/atom (~220 GPa). c, The band gaps calculated by DFT with the PAW potentials using VASP code (solid circles) and with pseudopotential method using ABINIT code (solid squares), and

by GW approximation with ABINIT (solid triangles) as a function of volumes for Na-oP8. With volume decreasing down to  $9.10 \text{ \AA}^3/\text{atom}$ , Na-oP8 starts to open up a band gap. However, at the volumes at which this structure is experimentally seen as stable ( $9.47\text{--}9.22 \text{ \AA}^3/\text{atom}$  from Ref. 8), Na-oP8 still remains weakly metallic (electronic density of states at Fermi level is rather small  $0.024 \text{ states}/(\text{eV}\cdot\text{atom})$  at the volume of  $9.21 \text{ \AA}^3/\text{atom}$ ). GW calculations for Na-oP8 were performed with 126  $k$  points in the first BZ and an energy cutoff of 15 Ry was chosen for the calculation of the Coulomb matrix. In the calculation of self-energy matrix, 36 occupied bands and 160 unoccupied bands were explicitly treated. With the choice of these parameters, the band gaps were found to converge within 0.01 eV.

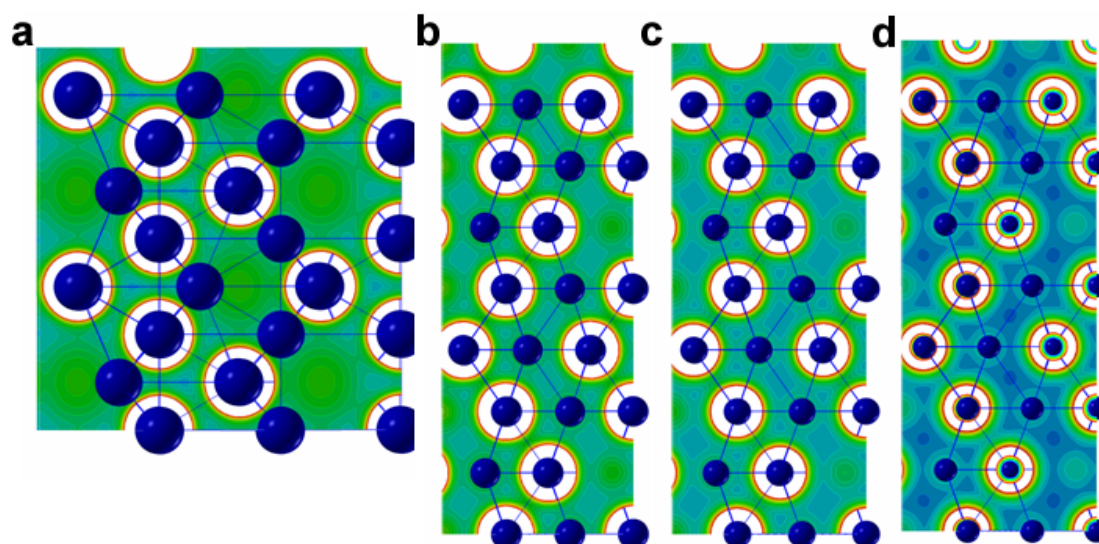


**Figure S6 | Valence electron densities in the (110) plane of (a) Na-hP4 at the volume of  $5.93 \text{ \AA}^3/\text{atom}$  ( $\sim 400 \text{ GPa}$ ), b) K-d.h.c.p at the volume of  $8.57 \text{ \AA}^3/\text{atom}$  ( $\sim 300 \text{ GPa}$ ), c) Rb-d.h.c.p at the volume of  $12.23 \text{ \AA}^3/\text{atom}$  ( $\sim 200 \text{ GPa}$ ), and d) Cs-d.h.c.p at the volume of  $19.45 \text{ \AA}^3/\text{atom}$  ( $\sim 100 \text{ GPa}$ ). The pressure values in the bracket are from theory. Density isocontours are drawn at intervals of  $0.05 \text{ e\AA}^{-3}$  colour-coded from 0 (blue) to  $1 \text{ e\AA}^{-3}$  (red). Interstitial charge concentrations are very strong in Na and get progressively weaker in K, Rb, and Cs.**

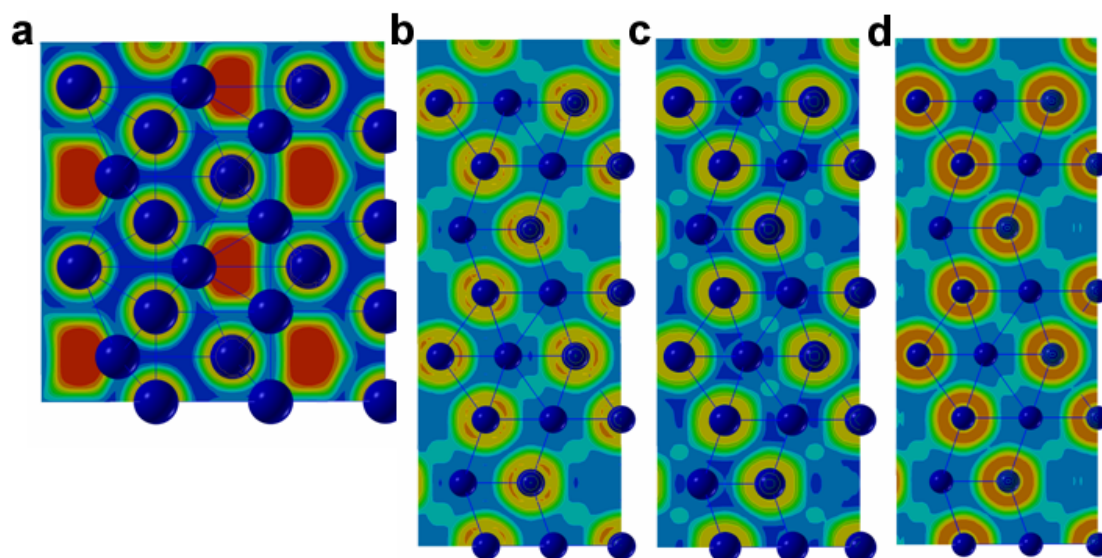


**Figure S7 | Valence electron localization function (ELF) in the (110) plane of (a) Na-hP4 at the volume of  $5.93 \text{ \AA}^3/\text{atom}$  ( $\sim 400 \text{ GPa}$ ), b) K-d.h.c.p at the volume of  $8.57 \text{ \AA}^3/\text{atom}$  ( $\sim 300 \text{ GPa}$ ), c) Rb-d.h.c.p at the volume of  $12.23 \text{ \AA}^3/\text{atom}$  ( $\sim 200 \text{ GPa}$ ), d) Cs-d.h.c.p at the volume of  $19.45 \text{ \AA}^3/\text{atom}$  ( $\sim 100 \text{ GPa}$ ). ELF (A. D. Becke and K. E. Edgecombe, *J. Chem. Phys.* 92, 5397 (1990)) is a local electrons pair probability for identification of localized electronic groups, and a dimensionless, empirical function in 3-space that generates relatively large values ranging between 0.5 and 1.0 in regions that can be ascribed to bonding and nonbonding localized electrons and smaller values (less than 0.5) where one expects the electrons to be delocalized. The pressure values in the bracket are from theory. ELF isocontours are drawn at intervals of 0.05 and colour-coded between 0 (blue) to 1 (red). Interstitial ELF maxima are pronounced in Na, but practically absent in K, Rb, and Cs.**

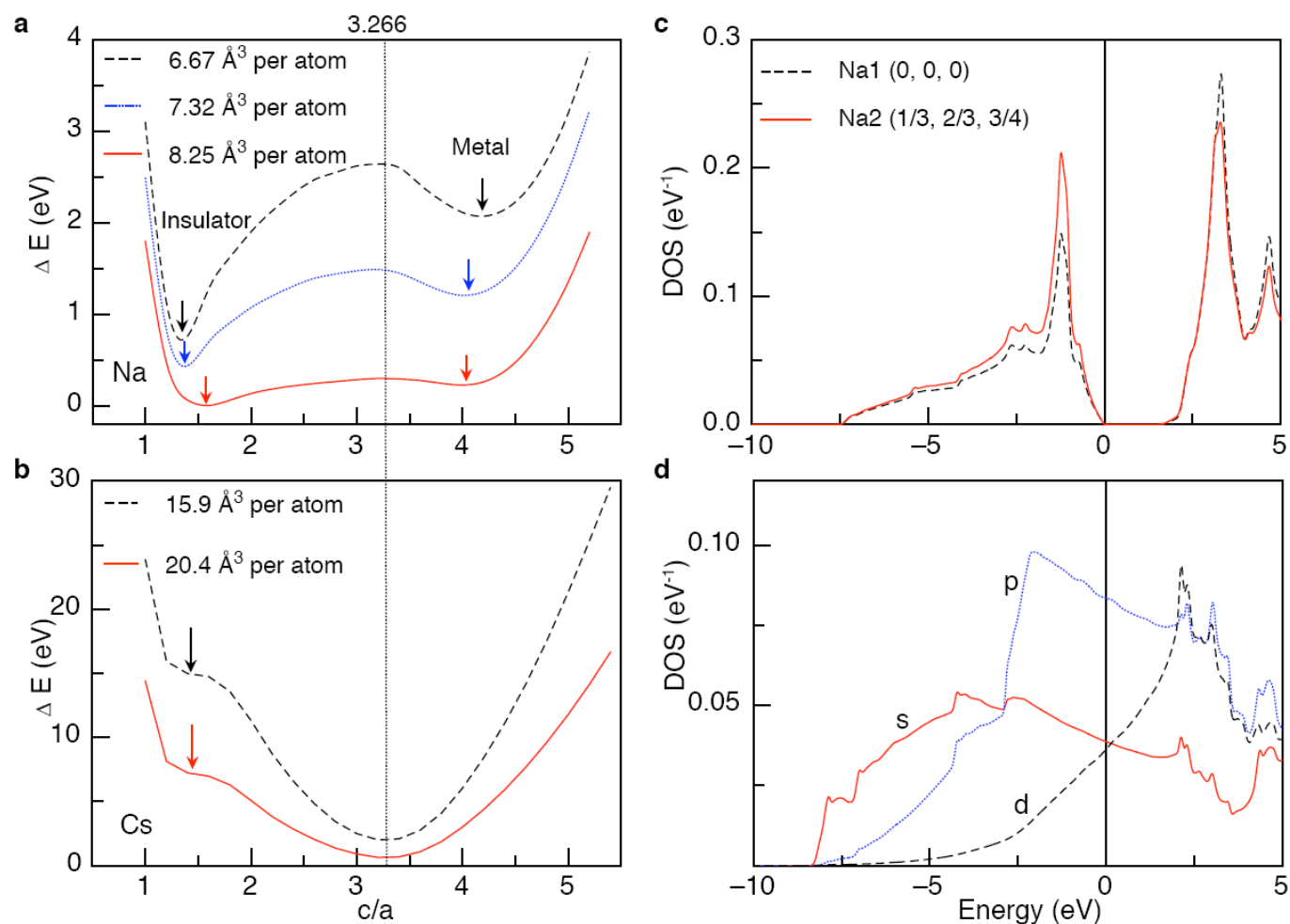


**Figure S8 | Electronic properties of Na-hP4 and Cs-d.h.c.p.** Total energies versus the  $c/a$  ratio for Na-hP4 (a) and Cs-d.h.c.p (b) at the selected volumes. For clarity, the energy curves were shifted by constant values. c, The total electronic DOS for the two inequivalent atomic sites in Na-hP4 at the volume of 6.67  $\text{\AA}^3$ /atom ( $\sim 300$  GPa). Weak ionicity is thus revealed by evidence of Na1-Na2 charge transfer. d, The partial DOS for the metastable metallic state of Na at  $c/a = 4.4$  at the volume of 6.67  $\text{\AA}^3$ /atom ( $\sim 300$  GPa). Two minima in the total energy profiles are revealed for Na-hP4, in which the stable state at  $c/a = 1.4$  is insulating, while the metastable state at  $c/a = 4.4$  is a good metal. This shows a close link between the insulating state and the abnormally low  $c/a$  ratio.

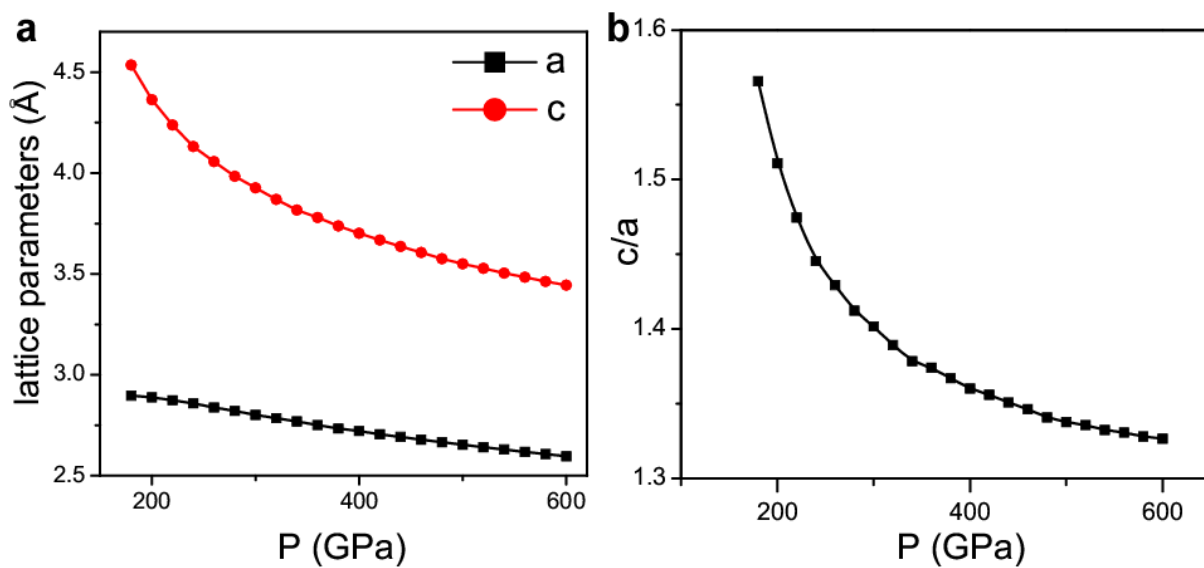


**Figure S9 | Lattice parameters with pressure for Na-hP4.** The anomalously small  $c/a$  ratio becomes even smaller on increasing pressure. This implies a larger distortion (relative to the ideal d.h.c.p structure) with stronger electron localization, which is responsible for the increase of the band gap with pressure.

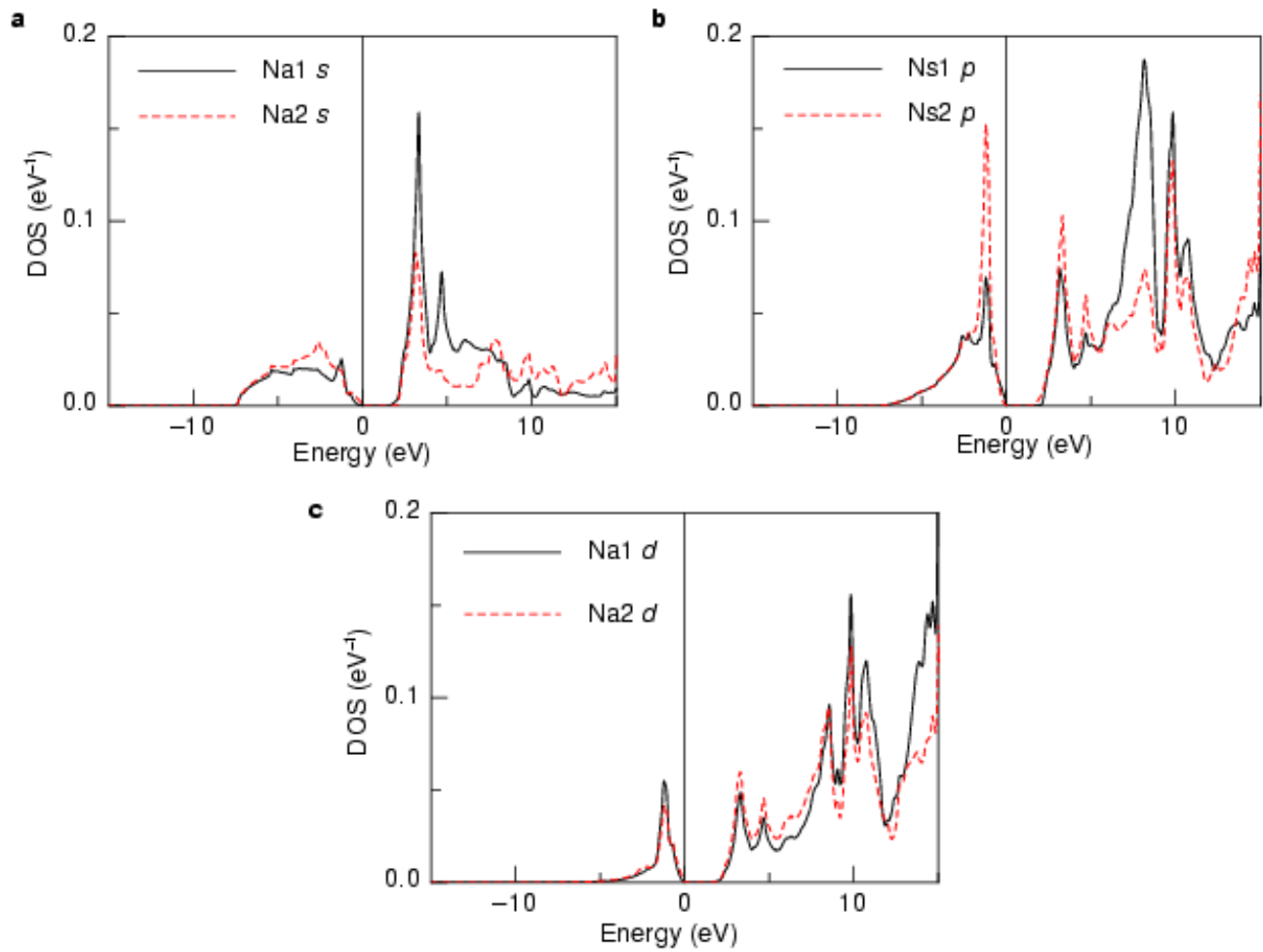


**Figure S10 | Projected density of states for two inequivalent Na atomic sites Na1 (0, 0, 0) and Na2 (1/3, 2/3, 3/4) in Na-hP4 at the volume of 6.50 Å<sup>3</sup>/atom (~320 GPa). a, b, and c are the *s*, *p*, and *d* contributions, respectively.**